analytical chemistry

Article

pubs.acs.org/ac

Pressure-Assisted Selective Preconcentration in a Straight Nanochannel

Anne-Claire Louër,*[,†] Adrien Plecis,[‡] Antoine Pallandre,[§] Jean-Christophe Galas,[†] André Estevez-Torres,[†] and Anne-Marie Haghiri-Gosnet[†]

[†]Laboratoire de Photonique et de Nanostructures, CNRS—UPR 20, 91460 Marcoussis , France

[‡]Elvesys, Pépinière Paris Santé Cochin, 75005 Paris, France

[§]Faculté de Pharmacie, Université Paris Sud, CNRS—UMR 8612, 92296 Châtenay-Malabry, France

Supporting Information

ABSTRACT: We investigate the preconcentration profiles of a fluorescein and bovine serum albumin derivatized with this fluorescent tag in a microfluidic chip bearing a nanoslit. A new preconcentration method in which a hydrodynamic pressure is added to both electroosmotic and electrophoretic contributions is proposed to monitor the location of the preconcentration frontline. A simple predictive model of this pressure-assisted electropreconcentration is proposed for the evolution of the flow profile along this micro/nano/microfluidic structure. We show with a small analyte such as fluorescein that the additional hydrostatic pressure mode enables to stabilize the concentration polarization (CP) effect, resulting in better control of the cathodic focusing (CF) peak. For BSA (bovine serum albumin), we exhibit that the variation of the hydrodynamic pressure can have an even more drastic effect on the preconcentration. We show that, depending on this hydrodynamic pressure, the preconcentration can be chosen, either in the cathodic side or in the anodic one. For the first time, we prove here that both anodic focusing (AF) and cathodic focusing (CF) regimes can be reached in the same structures. These results also open new routes for the detection and the quantification of low abundance biomarkers.

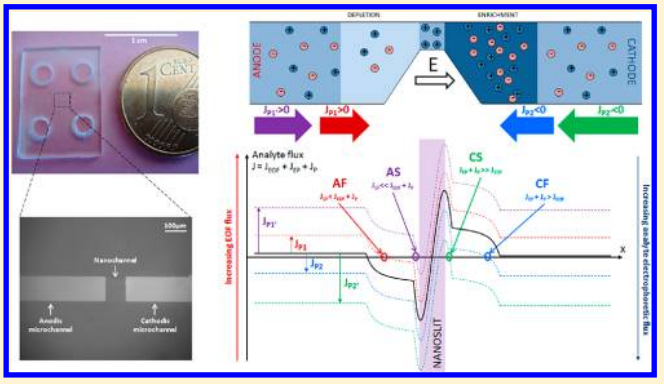

The transport of liquid in channels of nanometer size represents a growing practical and fundamental interest among researchers.[1−3] In such a nanofluidic channel where the role of the surface charge is exacerbated, the distribution of the charge is governed by the complex exchanges between the fluid and the surface.[4] The small dimension of the nanoslit renders the theoretical predictions and experimental discussions specific compared to the classical microfluidic field.[5−8] Electropreconcentration based on nanofluidic devices appears as an alternative approach to selectively detect low abundant biomarkers inside a complex solution.[9] The first preconcentration attempts on microfluidics were carried out by filtration through charge-selective nanoporous membranes.[10,11] However, to reduce aging effects, advanced nanofabrication techniques have been used to get more robust nanochannel structures with high aspect ratios. The height of the fluidic nanoslit can be of the size of the thickness of the electric double layer (EDL) over a length of several hundred micrometers or even millimeters.[12] In such a fluidic nanoslit, the unbalanced ionic transport between anionic and cationic species produces an enrichment-exclusion effect at both sides that is called the ion concentration polarization (CP) phenomenon.[13−15] This CP effect generates enrichment and depletion fronts in the background electrolyte, generating zones with respectively high and low conductivities. These conductivity gradients and the corresponding gradients in the local electromigration velocity of analytes allow focusing at the interfaces of enrichment and depletion fronts, similar to the mechanism of field amplified sample stacking (FASS).[16] Thus, CP enables electrokinetic trapping of analytes at the nanochannel entrance in both anodic and cathodic microchannel reservoirs that can be used for preconcentration.

Various preconcentration experiments have been reported,[14−23] and differences in the preconcentration factors and dynamics have been observed due to the large number of experimental parameters that have to be controlled. Previous theoretical works have tried to evaluate the efficiency of the electropreconcentration as a function of the electrokinetic properties of both the biomolecule and the buffer solution.[14,15,22] However, very few studies have been proposed for taking into account the influence of the embedding microchannel parts. Within a straight microchannel/nanoslit/microchannel (MNM) device, Santiago et al.[14] have identified two

Received: June 10, 2013
Accepted: July 22, 2013
Published: July 22, 2013

dx.doi.org/10.1021/ac4016159 | Anal. Chem. 2013, 85, 7948−7956

CP regimes: CP with propagation within both enrichment and depletion shocks moving away from the nanoslit during preconcentration, and CP without propagation for which polarization effects stay localized in the vicinity of the nanochannel. They also demonstrated that the two key parameters for CP are the nanochannel inverse Dukhin number based on reservoir concentration and the ratio of electrophoretic velocity of co-ions to electroosmotic velocity. In our laboratory, we have also previously demonstrated that the competition between the electroosmotic dragging force and the highly nonlinear electrophoretic forces induced by the nonpropagating CP effect is responsible for four preconcentration regimes.[22] Electrostatic exclusion is responsible for the stacking (S) regimes for which preconcentration occurs in the vicinity of the nanoslit entrance, while the concentration polarization (CP) effect produces the focusing (F) regimes for which preconcentration occurs at several hundred micrometers from the slit entrance. The stacking regime results from electrostatic exclusion of ions from the nanochannel, whereas the focusing regime results from the gradient in electromigration velocities of ionic species induced by the conductivity gradient at either the enrichment or the depletion front. Both of these regimes can occur either at the interface of the enrichment front (or shock) in the electrophoretically dominated regime or at the interface of the depletion front in the electroosmotically dominated regime. It is important to note that, in methods such as field amplified sample stacking (FASS)[16] and isotachophoresis (ITP),[24,25] both anions and cations can be separated without modifying the surface charge. The electropreconcentration through a MNM structure is a less complex method but requires different surface charge densities to separate simultaneously anions and cations. In this study, focusing of only anionic species will be evaluated. Since both the surface and the analytes are negatively charged, anionic analytes will focus on the cathodic side in electrophoretically dominated regime resulting in a "cathodic regime" or on the anodic side in an electroosmotically dominated "anodic regime". In the electroosmotically dominated regime at a moderate or high ionic strength (>10 mM), we also predicted that the highest preconcentration rate is observed for the anodic focusing regime of analytes with an electrophoretic mobility lower than 10^{-8} $m^2 \cdot s^{-1} \cdot V^{-1}$.[22] Those simulations allow a better understanding of the preconcentration efficiency as a function of the electrophoretic mobility of the analyte, the ionic strength of the solution, and the analyte charge. Beyond the unification of the different preconcentration regimes, this study also pointed out the strong dependence of such processes on the nature of the preconcentrated analytes. To summarize, one analyte at a certain concentration in one solution will preconcentrate at one precise location that corresponds to one of these four predicted regimes.

To choose selectively the location of the focal point, we propose in this paper a new protocol in which a hydrodynamic pressure is added to both electroosmotic and electrophoretic flows. This new pressure-assisted electropreconcentration is shown to monitor the location of the preconcentration frontline in either the anodic or cathodic microchannel reservoir. Similarly, White et al.[26] have recently observed a significant modulation of the CP due to the application of an additional pressure in glass nanopores with radii of around 200 nm. In this paper we will thus discuss the role of such additional pressure on CP affecting both focusing (F) and stacking (S) regimes.

MECHANISM OF PRESSURE-ASSISTED SELECTIVE PRECONCENTRATION

Compared to traditional electropreconcentration that is governed by the electric field, an external hydrodynamic pressure is here applied through the nanochannel. In addition to the two electroosmotic (J_{EOF}) and electrophoretic (J_{EP}) flows that are competing through the CP effect, the hydrodynamic flow ($J_{pressure} = J_P$) enables shifting the natural position of the focal point of the molecule in a direction that depends on the direction of the applied pressure. Thus, whereas in a simple electropreconcentration nanodevice the flux, that is the product of the analyte velocity with the section area S, is given by $J = SV = J_{EOF} + J_{EP} = (\mu_{EOF} + \mu_{EP})ES$, our new method is based on a total flow given by $J = SV + J_P = J_{EOF} + J_{EP} + J_P$ where the additional hydrodynamic flow J_P can take positive or negative values.

As previously mentioned, for traditional electropreconcentration the competition between electroosmotic (J_{EOF}) and electrophoretic (J_{EP}) flows through the CP effect has been described theoretically. In the case of a model solution containing only an ion and its co-ion, the two key parameters identified by Santiago et al.[14] are as follows:

1. The first parameter is an inverse Dukhin number, which describes the ratio of bulk conductivity to EDL conductivity, defined by $c_r^* h_n^* = (\nu_1 z_1 - \nu_2 z_2) F h_n c_r / (-2\nu_1 \sigma)$, where ν_i and z_i are respectively the mobility and the valence number of the ith ion (1 for the ion and 2 for the co-ion), F is the Faraday number, h_n is the nanochannel height, σ is the surface charge, and c_r is the concentration of the co-ion in the reservoir. This parameter is the product of the normalized concentration c_r^* and the normalized nanoslit height over the typical Debye length $h_n^* = h_n/\lambda_D$.

2. The second parameter is the ratio of the velocity of co-ions to the electroosmotic velocity $\nu_{2n} = \nu_2 z_2 F \eta / \zeta_n \varepsilon$, where ζ_n is the zeta potential value assumed to be uniform along the structure, η is the viscosity, and ε is the permittivity.

High values of $c_r^* h_n^*$ and low values of ν_{2n} favor CP without propagation[14,15] for which polarization effects stay localized in the vicinity of the nanochannel producing a stable focalization point. We can predict that, while the ionic strength can play a significant role in the first parameter, also presented in a previous publication as the volumic surface charge parameter,[27] an additional hydrostatic pressure will mainly modify the second parameter and could affect the CP effect.

In this paper, we study two cases representative of most of the previously reported experiments. For anionic dyes such as fluorescein and at low ionic strength ($\mu_{EP} = -3.5 \times 10^{-8}$ $m^2 \cdot V^{-1} \cdot s^{-1}$ [28,29]), preconcentration is dominated by the electrophoretic (J_{EP}) flow, which means that the focalization will generally be located in the cathodic reservoir (electrophoretically dominated regimes $J_{EP} \gg J_{EOF}$) and that an additional hydrostatic pressure will have a limited influence on the preconcentration effect. For negatively charged proteins such as bovine serum albumin (BSA) under the current experimental conditions in salted buffers at moderate ionic strength ($\mu_{EP} = -2.4 \times 10^{-8}$ $m^2 \cdot V^{-1} \cdot s^{-1}$ [30]), the electrophoretic and electroosmotic contributions are more equilibrated, which explains that the preconcentration could be observed either in the cathodic reservoir ($J_{EP} > J_{EOF}$) or in the anodic reservoir (electroosmotic dominated regime $J_{EP} < J_{EOF}$). One can expect that the additional hydrostatic pressure will exhibit a stronger influence on the preconcentration.

dx.doi.org/10.1021/ac4016159 | Anal. Chem. 2013, 85, 7948−7956

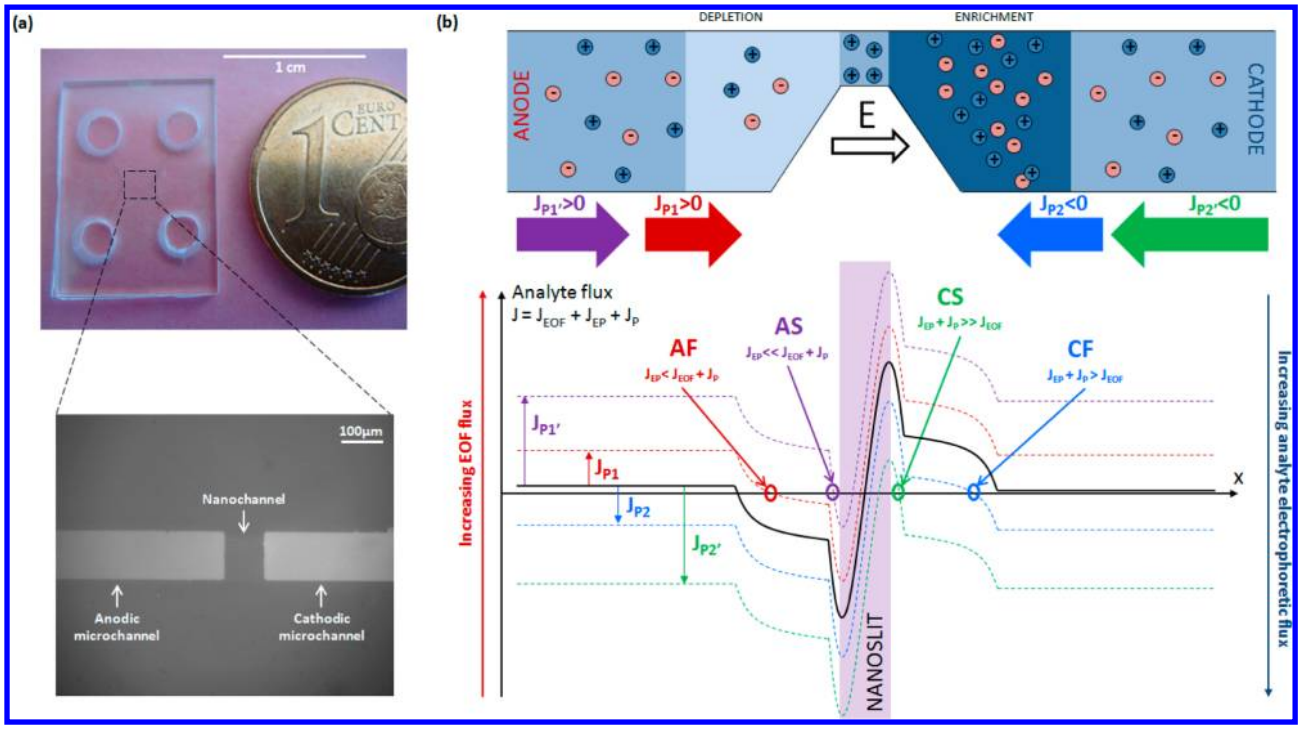

Figure 1. (a) Optical micrograph of the whole pure-glass chip that integrates a 100-μm-long and 150-nm-deep nanochannel in a 1-μm-deep microchannel. (b) Mechanism of pressure-assisted preconcentration and separation. The local transport rate profile is represented in the MNM structure (flux of the analyte vs distance in the structure). The black curve corresponds to the classical preconcentration of a protein when an electric field is applied. Four other cases are depicted: two cases with the application of a positive pressure (from the anode to the cathode) which has the effect of moving up the curve in the diagram and obtaining the two anodic regimes depending on the value of the pressure (anodic stacking (AS) in purple and anodic focusing (AF) in red); two cases with the application of a negative pressure (from the cathode to the anode) which has the effect of moving down the curve and obtaining the two cathodic regimes (cathodic stacking (CS) in green and cathodic focusing (CF) in blue).

We describe below the geometry of our device and the principle of our pressure-assisted electropreconcentration method. Our concentrator/separator integrates a depth restriction between two straight microchannels that corresponds to a nanoslit located at the channel center. Figure 1a gives a general description of the design of the whole MNM device. To better understand what happens in this straight MNM device, where both the electric field and the additional pressure are applied, Figure 1b describes the selective preconcentration principle. The evolution of the local transport rate profile in the MNM structure is reported for different cases. We will use the notations "classical" or "conventional" when preconcentration occurs after the application of an electric field, in the absence of a hydrodynamic pressure (J_P = 0). The black curve corresponds to the classical preconcentration of an analyte with a low electrophoretic mobility in a background electrolyte of a moderate ionic strength and under the application of an electric field. Due to the Donnan potential and the depletion/enrichment effect, the local flow exhibits this particular shape that has been previously determined through simulations.[22] At the intersection with the x-axis, where the flow velocity of the analyte becomes zero, the preconcentration occurs and this location is named the "preconcentration focusing point". For example, this specific localization arises in the anodic microchannel for the conventional electropreconcentration of BSA in a buffered solution at moderate ionic strength.[22]

If a positive hydrodynamic pressure is added in the same direction as the electric field from the anode to the cathode ("anodic pressure"; see red arrow in Figure 1b), the profile moves up. In fact, adding pressure in this direction means strengthening the effect of the electroosmotic flow (EOF). Such an increase in the applied pressure produces a preconcentration in the anodic focusing (AF) regime as shown by the red circle on the red dashed profile in Figure 1b. If the additional anodic pressure is still increased, the anodic stacking (AS) regime will be observed as described by the purple circle in Figure 1b. To conclude, for a protein at moderate ionic strength, an anodic positive pressure favors the two anodic AF and AS regimes by a simple enhancement of the EOF contribution.

In the case of additional pressure applied in the opposite direction from the cathode to the anode (named "cathodic pressure" in the following; see green and blue arrows in Figure 1b), the trend is reversed since the cathodic pressure reduces the role of EOF flow by promoting the electrophoretic component. The profile moves down. By applying this cathodic pressure, the two cathodic regimes (CF for cathodic focusing and CS for cathodic stacking) are observed. Again, preconcentration will not be possible for too-high values of pressure. Remember here that focusing regimes (AF or CF) correspond to focal points that extend far from the slit, whereas stacking regimes (AS and CS) produce preconcentration at the entrance of the nanoslit as previously predicted.[22] This new protocol for assisted-by-pressure electropreconcentration will allow choosing the localization of the preconcentration without suffering from the imposed regime. For BSA these two anodic and cathodic regimes have been observed as described in the section Pressure-Assisted Electropreconcentration of BSA:

dx.doi.org/10.1021/ac4016159 | Anal. Chem. 2013, 85, 7948−7956

Influence of the Additional Hydrodynamic Pressure on the Electroosmotically Dominated Regime.

For fluorescein at low ionic strength, electropreconcentration is dominated by the electrophoretic component producing a cathodic regime. Similarly as for BSA, adding a cathodic pressure (from the cathode toward the anode) will stabilize the preconcentration frontline in the cathodic microchannel in the vicinity of the nanoslit. In that case the initial curve (the black one) in Figure 1b will be positioned under the x-axis so that the preconcentration focal point will be in the cathodic reservoir (see green arrow in Figure 1b). For such an analyte with a very high mobility, only the cathodic CS regime is observable as it will be experimentally observed as described in the section Pressure-Assisted Electropreconcentration of Fluorescein: Influence of the Hydrodynamic Pressure on the Concentration Polarization Effect.

MATERIALS AND METHODS

Device fabrication, which consists of structuring a bottom wafer of glass to create the two microchannel reservoirs and the nanoslit, is based on standard photolithography and etching steps. A top glass is bonded to the bottom patterned glass substrate following a patented process.[31] The dimensions of the nanoslit in the concentrator are 100 μm length, 100 μm width, and 150 nm height. The other microchannels are 100 μm wide and 1.5 μm deep. The total length of the "H" is about 1 cm. The entire process is detailed in the Supporting Information (S1).

For preconcentration experiments, fluorescein and FITC-BSA (Sigma-Aldrich) were diluted in borate solutions with different ionic strengths that were buffered at pH 10. The external voltage for the electrophoretic component was generated by a dc Keithley 238 power supply associated with a Keithley 7001 multiplexer. The additional hydrodynamic pressure was applied through an ELVEFLOW AF1 pressure generator, while sequential injection and flow stop were achieved with an ELVEFLOW Multiplexer. Two channel cleaning processes were performed before each experiment. First, a cleaning of each new chip consisted of several consecutive channel rinses with different solutions: 10 min with 1 M sodium hydroxide solution, 10 min with the same solution diluted to 0.1 M, 15 min with water, and 2 h with the buffer solution. The second cleaning provided the same initial state before each application of electric field and pressure. It was composed of three steps: (i) an electric cleaning by applying 20 V for 2 min, (ii) an hydrodynamic injection of liquid for 10 min to renew the solution into the device, and (iii) a setting of pressure in the four tanks for 10 min. The injection of the analyte solution, made using a syringe, consisted of filling the four reservoirs so that the initial concentration of analyte was the same in the whole device. For imaging, we used an inverted fluorescent microscope (Axiovert 200, Zeiss), a mechanical shutter (Uniblitz VCMD1), and a CCD camera (Orca-ER, Hamamatsu). Images were captured at regular intervals during preconcentration experiments: every 30 s for 5 min for BSA and every second during 5 or 10 min for fluorescein. A Matlab program was developed for monitoring the fluidic setup during experiments. The fluorescence intensity was treated by another Matlab program that can extract and analyze fluorescence profiles. These profiles could be plotted as raw intensity data, but we decided here to rather relate them to the protein concentration in order to think in terms of factors of preconcentration. This experimental pathway is detailed in the Supporting Information (S2).

RESULTS AND DISCUSSION

Pressure-Assisted Electropreconcentration of Fluorescein: Influence of the Hydrodynamic Pressure on the Concentration Polarization Effect. Our previous numeric calculations[22] have shown that fluorescein diluted at low KCl concentrations (down to 10 μM) corresponds to a cathodic regime. We can expect the cathodic focusing (CF) profile to be unstable over time especially for high surface charge (at very low ionic strength) and high electric fields. Due to a significant electroosmotic flow, the concentration polarization propagates toward the cathode, which is the direction of the EOF transport. Such an unstable CF preconcentration profile also corresponds to low values of $c_r{}^*h_n{}^*$ for a propagating CP as predicted by Santiago et al.[14] In both predictions, a stable CF profile can be observed when decreasing the external voltage or surface charge, or at higher values of $c_r{}^*h_n{}^*$ in the nonpropagating CP regime. This stable CF regime corresponds to an electrophoretically dominated regime.

To keep the same surface charge allowing maintaining $\nu_{2n} = \nu_2 z_2 F\eta/\zeta_n\varepsilon$ at the same value, a constant external field E = 80 V/cm was applied for all experiments with fluorescein. The initial concentration of fluorescein was maintained at 10 μM, and supporting buffered borate solutions were chosen so that the pH of the solution remained close to 10. Only the ionic strength of the borate buffer was varied from 50 μM to 1 mM, which should result in a decrease of the surface charge at high ionic strength (and a decrease of $c_r{}^*h_n{}^*$).

Figure 2a gives experimental preconcentration profiles for two conventional cathodic preconcentrations (in the absence of a hydrodynamic pressure $J_P = 0$). The fluorescein concentration as a function of the distance from the nanoslit is presented at different preconcentration times. At very low ionic strength (50 μM) for which exclusion enrichment in the nanochannel is maximal, there is no stable preconcentration. The concentration begins to sharply rise, reflecting a preconcentration, but after 3 min, it decreases while the peak shifts far from the nanoslit toward the cathode due to a nonnegligible EOF component. Such a preconcentration profile resembles the unstable CF in the propagating CP that is expected at high surface charge (low ζ_n) and low $c_r{}^*h_n{}^*$.[15,22] Increasing the ionic strength of the buffer to 300 μM stabilizes the CS peak since after 5 min the preconcentration moves only several hundred micrometers from the nanoslit. Also the concentration does not decrease in 5 min, which reflects a stable CF regime. This is in line with Santiago predictions since increasing the ionic strength corresponds to a $c_r{}^*h_n{}^*$ increase due to an enhancement of $h_n{}^*$ with a Debye length that is largely reduced. In the ($c_r{}^*h_n{}^*$, ν_{2n}) phase diagram,[15] such a stable CF point corresponds to the nonpropagating CP. Finally, we also observe that the larger the ionic strength the closer to the nanoslit the stable CF point is (see the Supporting Information, S3, for experimental preconcentration profiles recorded at higher ionic strength from 3 mM to 100 mM). This is also in line with previous results and shows that the lower the ionic strength is, the stronger the volumic surface charge is[27] and the larger will be the CP region until a propagation of this CP region occurs. At very low ionic strengths, the CP generation capability of the nanoslit is maximal, and the number of ionic species in the microchannels is too low to sustain the charge selectivity of the nanostructure, which then results in a

dx.doi.org/10.1021/ac4016159 | Anal. Chem. 2013, 85, 7948−7956

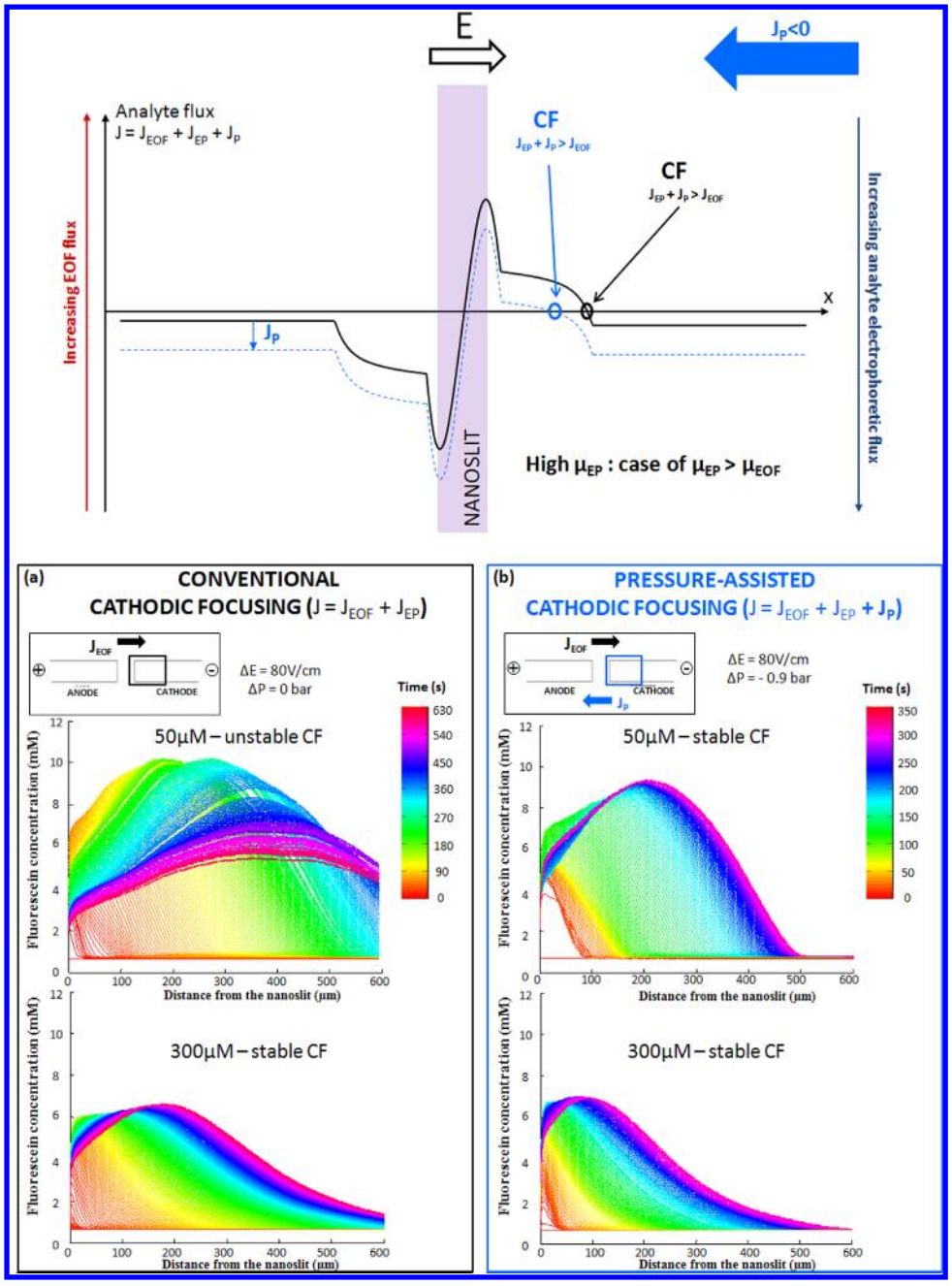

Figure 2. Role of ionic strength of the buffer solution in selective preconcentration of fluorescein: (a) conventional electropreconcentration compared to (b) cathodic pressure-assisted electropreconcentration.

propagating CP region. The maximal value of the preconcentration rate is about 10^3 for the lower ionic strength. With a quite large nanoslit height (h = 150 nm), this rate is also in line with previous experiments.[22]

Let us now consider the same experiment with an additional 0.9 bar hydrodynamic pressure applied from the cathode to the anode (Figure 2b). For a low ionic strength (50 μM), the additional hydrostatic pressure is responsible for a stabilization of the fluorescein preconcentration front, which can also be interpreted as a transition from a propagating CP to a nonpropagating CP. This result shows that hydrostatic pressure can play a significant role in the CP effect and can be used to tune and stabilize this effect. This influence of additional flows on CP effect was also commented on by Wang et al.,[17] who observed a propagating CP in their structures, while a stable CP region could be obtained when they added a transverse EOF flux in their "H shape" device.

For higher ionic strengths, the hydrostatic pressure also plays a role in the preconcentration profile and seems to compress the preconcentration front toward the nanoslit in the same direction as the additional hydrostatic flow. The cathodic-pressure-assisted electropreconcentration scheme (green and blue pressure arrows in Figure 1b) has been reported in the top of Figure 2 to comment on the effect of the additional pressure on the preconcentration. The black curve in this diagram corresponds to the classical preconcentration without pressure. It is located below the vertical axis for flow (J = 0) since the electrophoretic flux dominates, producing the cathodic focusing (CF) profile. Adding a cathodic pressure shifts this profile toward negative values as shown on the blue curve, which can

dx.doi.org/10.1021/ac4016159 | *Anal. Chem.* 2013, 85, 7948–7956

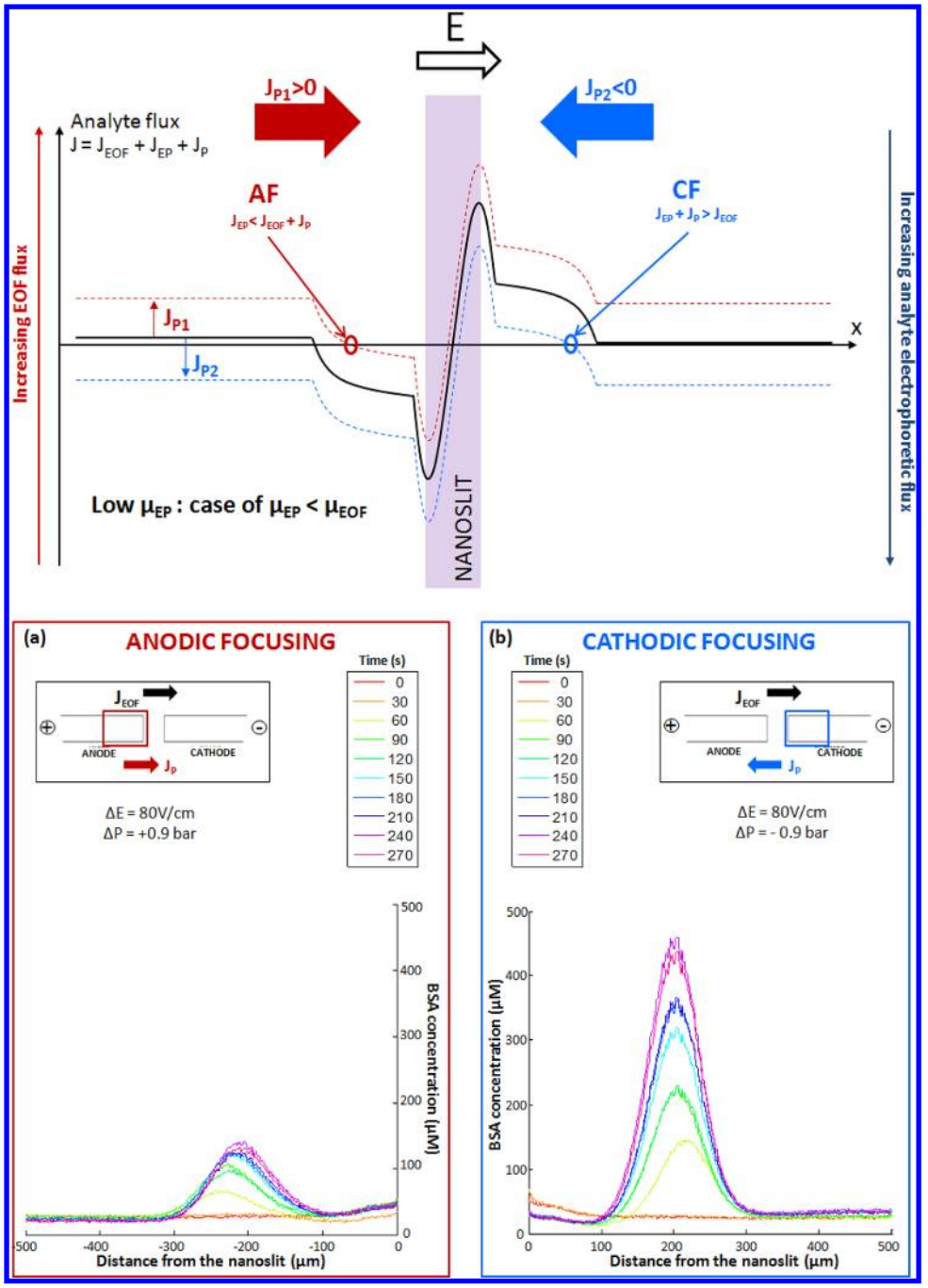

Figure 3. Two types of preconcentration for BSA: (a) anodic focusing (AF) when voltage and pressure are applied in the same way corresponding to an "anodic pressure" and (b) cathodic focusing (CF) when the two flows are opposite (case of a "cathodic pressure"). ΔE = 80 V/cm and $\Delta P = \pm 0.9$ bar.

explain this preconcentration frontline migration toward the nanoslit. In this blue curve, there is no need for a CP region modification to explain this shift. However, this interpretation should also result in an increase in the total flux of fluorescein that should be observable in the preconcentration rate. As this preconcentration rate remains almost stable, another interpretation for this shift in the preconcentration frontline can be proposed on the basis of a negligible shift of the global flux line but a significant compression of the CP region toward the nanoslit.

To conclude, the addition of a cathodic pressure on the preconcentration of fluorescein demonstrates that CP can be controlled and the preconcentration front can be modulated and stabilized in space using an additional hydrostatic pressure. On the other hand, the additional hydrostatic pressure barely affects the preconcentration rate, which can be explained by the fact that the preconcentration remains mainly dominated by electrophoretic flux for fast migrating analytes.

Pressure-Assisted Electropreconcentration of BSA: Influence of the Additional Hydrodynamic Pressure on the Electroosmotically Dominated Regime. In this section, we consider the pressure-assisted preconcentration at moderate ionic strength in electroosmotically dominated regimes using BSA, which is a protein with a lower

dx.doi.org/10.1021/ac4016159 | *Anal. Chem.* 2013, 85, 7948−7956

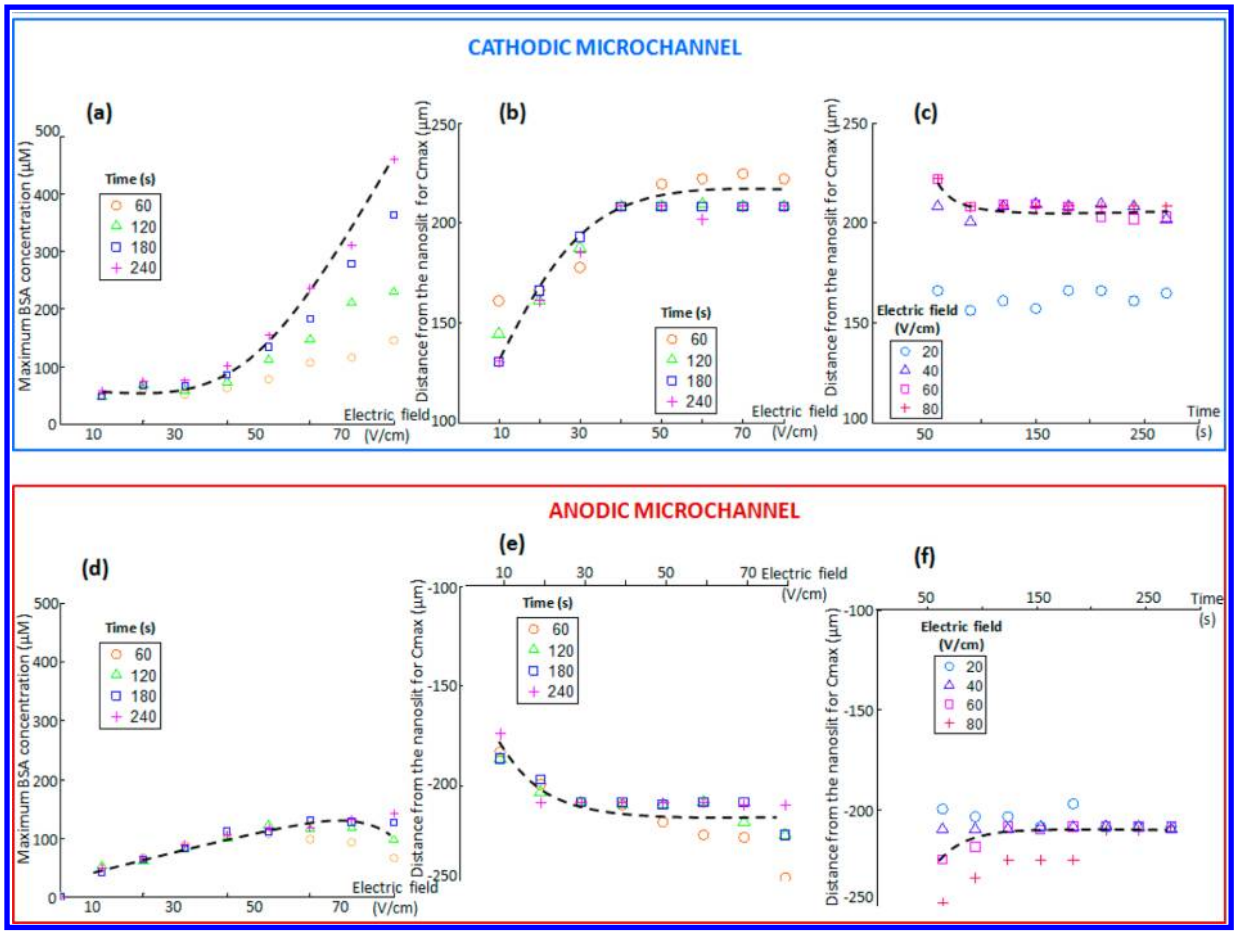

Figure 4. (a and d) Evolution of maximum BSA concentration as a function of the electric field for four different times. A maximum can be observed for the anodic regime, whereas an unsatured regime and higher rates of preconcentration are observed for the cathodic one. (b and e) Evolution of the location of the preconcentration peak as a function of the electric field for four different times. The peak is extremely stable in time at high voltage (E > 40 V/cm). (c and f) Evolution with time of the location of the preconcentration peak for four different electric fields. Dashed curves are guidelines to figure out the evolution of each studied parameter.

electrophoretic mobility than that of fluorescein. BSA has been diluted in a 50 mM borate buffer solution at pH 10 at a concentration of 1.5 μM. Similarly to fluorescein experiments, an electric field of 80 V/cm and a pressure of 0.9 bar were also applied for BSA pressure-assisted electropreconcentration. For such a protein with a low mobility, the classical preconcentration should occur in the anodic microchannel of the device.[22] We have also simplified the schematic diagram of Figure 1b for this specific case and the new diagram is presented at the top of Figure 3. The black curve in this diagram that corresponds to a classical preconcentration without pressure is here located above the vertical axis for flow (J = 0) since the EOF component dominates, producing the anodic focusing (AF) profile. Let us now consider what happens experimentally with an additional pressure applied in the two directions. Figure 3 reports on two different pressure-assisted electropreconcentration experiments: in Figure 3a a positive hydrodynamic pressure is added in the same direction as the electric field from the anode to the cathode ("anodic pressure"; see red arrow) whereas in Figure 3b a "cathodic pressure" is applied in the reverse direction from the cathode to the anode (see blue arrow). The anodic pressure stabilizes the anodic focusing (AF) regime as shown in Figure 3a, whereas a stable cathodic focusing (CF) regime occurs for a cathodic pressure (Figure 3b). The intensity of fluorescence has been related to the corresponding BSA concentration to extract properly the value of the preconcentration factor (see Supporting Information, S2). Surprisingly, this preconcentration factor reaches a maximal c_m/c_0 value of 3×10^2 (with c_0 = 1.5 μM and c_m = 450 μM) for the cathodic focusing regime (Figure 3b).

The evolution of the maximum BSA concentration is reported in Figure 4a,d for the two cases of pressure-assisted preconcentration. Note that each color allows following the time dependence of the BSA concentration.

For the anodic focusing regime, the evolution of the BSA concentration as a function of the electric field (Figure 4d) exhibits a maximum value of about 130 μM at E = 70 V/cm (the corresponding preconcentration rate is almost 10^2). This optimal voltage was previously predicted for model KCl solutions[32] and was then explained by the nonlinear dependence of the preconcentration factor with regard to the electric field: the polarization process, which is responsible for a saturation of the current at high electric fields, induces a saturation of the electrophoretic component, while electroosmosis exhibits a quasi-linear dependence with the electric field. The increase of the applied voltage thus results in a continuous shift of the molecule flows toward EOF dominated regimes, and even if the global molecular flow toward the preconcentration zone increases, the CP barrier continuously

dx.doi.org/10.1021/ac4016159 | Anal. Chem. 2013, 85, 7948−7956

decreases until the CP region is no longer sufficient to stop the molecules before the nanoslit.

For the cathodic regime, the same dependence should also be observed (Figure 4a). We could not experimentally measure a maximum value of BSA concentration, but we expect that the optimal voltage should be higher than 80 V/cm. This result also confirms that the preconcentration window of the cathodic regime is larger than the anodic regime in our system, which is in agreement with a larger cathodic CP gradient.

In terms of preconcentration factors, the cathodic preconcentration is more efficient than the anodic regime. One can interpret this result as the fact that the cathodic CP region exhibits a stronger electric field gradient than the anodic one with borate buffers. This is not in agreement with simulations using KCl buffers,[22] where anodic regimes were supposed to provide higher preconcentration factors than cathodic regimes. Future experiments and simulations should tell if this is due to the additional pressure effect (the cathodic pressure reduces global EOF flow and then increases the CP gradient) or if this is due to mobility differences between positive and negative ions from borate solutions (that naturally enhance the cathodic CP with regard to the anodic CP).

These experiments demonstrate for the first time that both anodic and cathodic preconcentrations can be obtained simply by changing the direction of the additional pressure. In all cases and as observed for fluorescein experiments, this new protocol allows a better stabilization of the preconcentration frontline due to a reduction of EOF/electrophoretic flow coupling. In the case of MNM structures enabling both anodic and cathodic focusing regimes as reported in Figure 3, we observed that both preconcentration regimes seem pretty symmetric in terms of localization (distance from the slit). This result suggests that, for our structure and the buffer used, the CP region extends symmetrically in both directions of the nanoslit. Taking a look at Figure 4, we note that, for the two stable focusing regimes, the peak is remarkably stable over time. In Figure 4b,e, different colors have been used to follow the dynamics of the preconcentration. We note that for each applied electric field, as soon as the peak appears, it stays almost at the same position even after 5 min. Secondly, the value of the electric field impacts pretty slightly on the position of the peak (Figure 4c,f). Therefore, a very small shift of the peak position of about 60 μm is observed between the two extreme voltages. At voltages higher than 40 V/cm, whatever the applied electric field, the focusing frontline stays at the same position. This saturation distance is about 225 μm for the anodic profile and 210 μm for the cathodic profile. To conclude, the peaks are pretty stable over time and electric field for the two focusing regimes.

Both results suggest that, in the presence of an additional hydrodynamic pressure, the CP region is stabilized whatever the value of the applied voltage. In terms of application, this result means that the position of the preconcentration detection will vary very slightly even for long preconcentration experiments under high electric fields.

The repeatability of these experiments has to be commented on. If the electropreconcentration frontline position and the fluorescence intensity are reproducible day after day in the same MNM chip, we have observed some discrepancy from chip to chip. We assume that this discrepancy is related to two well-known experimental difficulties: (i) the height and the shape of the long nanoslit can slightly differ even if the glass chips are obtained from the same batch and (ii) the nanochannel surface charge is difficult to stabilize at a precise and reproducible value even if a 1 h reclean process is systematically used for each new MNM chip. As a conclusion, some of the MNM structures tested in this study exhibited the cathodic only focusing regime (whatever the additional pressure superimposed was, the preconcentration remained dominated by electrophoretic flow $J_P + J_{EOF} \ll J_{EP}$) and others exhibited anodic only focusing regimes ($J_P + J_{EOF} \gg J_{EP}$). In order to enable the additional Poiseuille flow and to always choose the type of preconcentration regime, the pressure range should be increased in future studies, or the geometry should be modified (for example, the length of the nanoslit should be decreased).

CONCLUSION

In this work, a novel protocol was proposed for the preconcentration of biomolecules under electrophoretic and hydrodynamic mixed regimes through a microchannel/nanoslit/microchannel chip. A simple model for the evolution of the flow profile allows predicting the role of the additional hydrodynamic pressure in the location of the preconcentration frontline. All fluorescence patterns are in good agreement with these predictions. Moreover, our experimental results obtained with fluorescein and BSA underline the benefit of applying such hydrodynamic pressure to stabilize and control the concentration polarization effect and to be able to control the selective preconcentration of analytes in terms of the preconcentration factor and localization as compared to pure electrical preconcentration. Another advantage of this preconcentration methodology is shown by the higher temporal stability of the analyte distribution close to the nanoslit which validates the reliability of this methodology for future biodetection studies.

Future experiments should investigate the selectivity that such a protocol can provide to complex biological mixtures. Indeed, we observed that, depending on the analyte, the optimal electric field and additional hydrostatic pressure as well as the preconcentration location could vary significantly. Such selective preconcentration systems could be applied to antigen/anibody complex detection or any electrophoretic based sorting technique with an unprecedented detection limit based on the preconcentration capability.

ASSOCIATED CONTENT

Supporting Information

Additional information as noted in the text. This material is available free of charge via the Internet at http://pubs.acs.org.

AUTHOR INFORMATION

Corresponding Author

*E-mail: anne-claire.louer@lpn.cnrs.fr.

Notes

The authors declare no competing financial interest.

ACKNOWLEDGMENTS

All authors would like to thank DGA (Direction Générale pour l'Armement—French Ministry of Defence) for the financial support of the Ph.D. grant of A.-C.L.

REFERENCES

(1) Abgrall, P.; Nguyen, N. T. *Anal. Chem.* **2008**, *80*, 2326.
(2) Eijkel, J. C. T.; van den Berg, A. *Microfluid. Nanofluid.* **2005**, *1*, 249.

(3) Schoch, R. B.; Han, J. Y.; Renaud, P. *Rev. Mod. Phys.* **2008**, *80*, 839.
(4) Yuan, Z.; Garcia, A. L.; Lopez, G. P.; Petsev, D. N. *Electrophoresis* **2007**, *28*, 595−610.
(5) Xuan, X.; Li, D. *Electrophoresis* **2007**, *28*, 627−634.
(6) Garai, A.; Chakraborty, S. *Electrophoresis* **2010**, *31*, 843−849.
(7) Movahed, S.; Li, D. *Electrophoresis* **2011**, *32*, 1259−1267.
(8) Conlisk, A. T. *Electrophoresis* **2005**, *26*, 1896−1912.
(9) Gervais, L.; de Rooij, N.; Delamarche, E. *Adv. Mater.* **2011**, *23*, H151−H176.
(10) Lee, B. Y.; Seo, S. M.; Lee, D. J.; Lee, M.; Lee, J.; Cheon, J.-H.; Cho, E.; Lee, H.; Chung, I.-Y.; Park, Y. J.; Kim, S.; Hong, S. *Lab Chip* **2010**, *10*, 894−898.
(11) Kuo, T. C.; Cannon, D. M.; Chen, Y. N.; Tulock, J. J.; Shannon, M. A.; Sweedler, J. V.; Bohn, P. W. *Anal. Chem.* **2003**, *75*, 1861−1867.
(12) Kuo, T. C.; Sloan, L. A.; Sweedler, J. V.; Bohn, P. W. *Langmuir* **2001**, *17*, 6298−6303.
(13) Plecis, A.; Schoch, R. B.; Renaud, P. *Nano Lett.* **2005**, *5* (6), 1147−1155.
(14) Ali, M.; Zangle, T. A.; Santiago, J. G. *Langmuir* **2009**, *25*, 3898−3908.
(15) Zangle, T. A.; Ali, M.; Santiago, J. G. *Langmuir* **2009**, *25*, 3909−3916.
(16) Bharadwaj, R.; Santiago, J. G. *J. Fluid Mech.* **2005**, *543*, 57−92.
(17) Wang, Y.; Stevens, A.; Han, J. *Anal. Chem.* **2005**, *77*, 4293−4299.
(18) Pu, Q.; Yun, J.; Temkin, H.; Liu, S. *Nano Lett.* **2004**, *4*, 1099−1103.
(19) Schoch, R. B. *Transport Phenomena in Nanofluidics: From Ionic Studies to Proteomic Applications*. Ph.D. Thesis, École polytechnique fédérale de Lausanne, Lausanne, Switzerland, 2006.
(20) Kim, S. M.; Burns, M. A.; Hasselbrink, E. F. *Anal. Chem.* **2006**, *78*, 4779−4785.
(21) Datta, A.; Gangopadhyay, S.; Temkin, H.; Pu, Q.; Liu, S. *Talanta* **2006**, *68*, 659−665.
(22) Plecis, A.; Nanteuil, C.; Haghiri-Gosnet, A.-M.; Chen, Y. *Anal. Chem.* **2008**, *80*, 9542−9550.
(23) Ko, S. H.; Song, Y.-A.; Kim, S. J.; Kang, K. H.; Han, J. *Lab Chip* **2012**, *12* (21), 4472−4482.
(24) Jung, B.; Bharadwaj, R.; Santiago, J. *Electrophoresis* **2003**, *24*, 3476−3483.
(25) Storey, B. D.; Tilley, B. S.; Lin, H.; Santiago, J. G. *Phys. Fluids* **2005**, *17*, 018103.
(26) Lan, W.-J.; Holden, D. A.; White, H. S. *J. Am. Chem. Soc.* **2011**, *133*, 13300−13303.
(27) Plecis, A.; Pallandre, A.; Haghiri-Gosnet, A. M. *Lab Chip* **2011**, *11*, 795−804.
(28) Milanova, D.; Chambers, R. D.; Bahga, S. S.; Santiago, J. G. *Electrophoresis* **2011**, *32*, 3286−3294.
(29) Bahga, S. S.; Bercovici, M.; Santiago, J. G. *Electrophoresis* **2010**, *31*, 910−919.
(30) Böhme, U.; Scheler, U. *Chem. Phys. Lett.* **2007**, *435*, 342−345.
(31) Nanteuil, C.; Haghiri-Gosnet, A.-M. (CNRS). Patent FR 1054183, May 28, 2010.
(32) Plecis, A.; Nanteuil, C.; Haghiri-Gosnet, A. M.; Chen, Y. *Proceedings of μTAS*; Chemical and Biological Microsystems Society: San Diego, CA, 2008; p 200.